Research Article

Study on Numerical Simulation of Fire Danger Area Division in Mine Roadway

Hu Wen [iD],[1,2] **Yin Liu** [iD],[1,2] **Jun Guo** [iD],[1,2] **Ze Zhang** [iD],[3] **Mingyang Liu** [iD],[1,2] **and Guobin Cai** [iD][1]

[1]*School of Safety Science and Engineering, Xi'an University of Science and Technology, Xi'an 710054, China*
[2]*Key Laboratory of Western Mine and Hazard Prevention, Ministry of Education of China, Xi'an 710054, China*
[3]*Xi'an Tianhe Mining Technology Co., Ltd, Xi'an 710000, China*

Correspondence should be addressed to Yin Liu; 18120089021@stu.xust.edu.cn and Ze Zhang; 592719251@qq.com

High-temperature poisonous smoke produced by coal mine roadway fire seriously affects miners' lives and safety. Studying the development law of high-temperature smoke in the process of mine roadway fire and then exploring the danger of roadway are of great significance to personnel safety and post-disaster rescue. In order to study this problem, the CFD numerical simulation method is used to establish a fire calculation model based on ANSYS Fluent software in the development stage of mine fire. The high-temperature flue gas flow in the roadway during the development stage of mine fire is simulated, and the variation law of temperature field and gas concentration field with time and space position under different levels of roadway in the development stage of fire is revealed. The variation rules of environmental parameters, such as temperature, CO, and CO_2, are obtained by numerical calculation. Based on these, the danger zones of smoke spread in fire development stage are divided by the critical values of high-temperature smoke and toxicity evaluation index, and the mathematical fitting analysis of the evolution of the dangerous area with time is carried out. The research results have certain theoretical guiding significance for reducing underground environmental pollution and ensuring the personal safety of workers and rescuers.

1. Introduction

As one of the five possible major mine disasters, mine fires are a serious threat to the safety of underground workers and industrial property [1–3]. Once a fire breaks out underground, the mine tunnel would form a high-temperature flue gas environment, which contains toxic asphyxiating gases (such as CO, CO_2, NO_x, HCL, Cl_2, H_2S, SO_2, and NH_3) and harmful smoke particles [4–6]. As the fire intensity increased during the fire development process, the mine ventilation network was destroyed, and the air flow temperature and pressure were changed [7, 8]. Because the mine tunnel is a confined space, the smoke and heat generated during the fire are difficult to discharge in time. Therefore, the high-temperature smoke diffuses rapidly in the tunnel, polluting the underground working environment and seriously threatening the lives of workers [9, 10]. However, due

to the inability to scientifically and rationally define dangerous areas, the evacuation of underground personnel and the implementation of emergency rescue operations is very difficult during underground mine fires [11, 12].

Many researchers have studied the spread of high-temperature smoke during mine fires to determine the associated danger, and they have obtained fruitful results. Since 1980s, scholars all over the world have studied the flow of smoke during tunnel fires and the impact of fire on mine ventilation systems through experimental tests and numerical simulations [13–15]. Xu et al. [16], Egan [17], Li [18], Li and Ingason[19], and Shafee and Yozgatligil [20] and other researchers have established a full-scale tunnel and different small-scale tunnels to carry out extensive fire testing and studied the evolution of environmental parameters such as temperature, CO, and CO_2 in the tunnel during the catastrophe, and a series of quantitative studies were carried out on the relationship between the

dimensionless smoke retreat length and the roadway wind speed and fire source. It is widely used in the numerical simulation of tunnel fire because the numerical simulation method has the characteristics of short test period, high efficiency, resource saving, and strong flexibility. For example, to study the distribution law of high-temperature gas and the influence of throttling in tunnel fire, Zhang et al. [15], Li et al. [21], Zhu et al. [22], Vaitkevicius and Carvel [23] considered different initial conditions and geometric factors of tunnel (height, slope, and radius of curvature). Fan et al. [1] and He et al. [24] employed the FDS numerical simulation to study the development characteristics of high-temperature smoke flow in tunnels under stable fire source power of 1 MW–20 MW and different ventilations. Chen et al. [25] regarded the fire source as a high-temperature flue gas release source with a fixed temperature of 2000 K and a fixed amount of gas release, and the distribution law of the temperature and toxic gases in the tunnel were explored to the danger of the tunnel. At present, numerous research works have been carried out on the development law of tunnel fire smoke flow, throttling effect, and other fire evolution characteristics. However, there are the relatively few studies on the distribution law of mine roadway fire smoke flow and the distribution characteristics of tunnel dangerous areas in the condition of unsteady fire source.

According to the investigation and analysis of the accident, the main causes of casualties caused by underground tunnel fire are toxic gas and high-temperature [26–28]. In this paper, the ANSYS Fluent15.0 was employed to simulate calculation of the changes of roadway temperature and smoke flow characteristics during the fire evolution in the small-scale straight tunnels, which used the $t2$ fire model to treat the fire source as a source term that changes with time, and set the toxic asphyxiant gas release source term. In addition, based on the foundation of previous studies, standards for dividing tunnel dangerous areas were established to monitor the changes of temperature and gas concentration in the tunnel and determined the distribution characteristics law of the fire dangerous area in the tunnel.

2. Numerical Simulation Method

Fluent and ICEM, as embedded modules of ANSYS third-party commercial software, are widely used in fluid calculation, heat transfer, and chemical reaction simulation. In this paper, the geometric model is established by ICEM, the fire source model is set by user-defined function (UDF), and the model is imported into FLUENT software to calculate the development law of high-temperature toxic smoke in roadway fire process.

2.1. Physical Model and Fire Source. The physical model is based on the geometric prototype of the small flat roadway fire test bench of Xi'an University of Science and Technology [18]. A geometric model with a ratio of 1 : 1 was established. The experimental roadway model is 11 m long, 0.6 m wide, and 0.4 m high. The roadway section has a continuous, constant arch. The fire source was set to a circular imprinted surface with a radius of 0.06 m, located bottom of roadway 1 m from the air inlet. Ten measuring points were laid along

the roadway model to monitor the simulation data results. These points were arranged in two layers along the central axis of the roadway and numbered as levels L_1 and L_2, respectively, which were 0.1 m and 0.2 m below the top of the tunnel arch. The concrete model is shown in Figure 1.

The commonly used formulas for calculating heat release rate of unsteady fire sources are t^2, complete development model, MRFC heat release rate calculation formula, and FFB index calculation model. t^2 fire is the most famous unsteady fire source, which is widely used in North America to describe the relationship between heat release rate and time during the development of fire [29–31]. In this paper, the t^2 model was used as the fire source term to calculate the temperature change during the fire process, and the fire source power is embedded in Fluent 15.0 [32] through UDF code of fire source power [33] for unsteady state numerical simulation calculation:

$$Q = bt^2, \tag{1}$$

where Q is the heat release rate in kilowatts, b is the development coefficient, taken as 0.0469 kW/s^{-2}, and t is the fire development time in seconds.

UDF code of fire source power [33]:

```
#include "udf. h"
DEFINE_PROFILE (unsteady_firesource, thread, p)/*
Define fire source power function name */
{
    face_t f;
    real a;
    begin_f_loop (f, thread)
        {
        t = RP_Get_Real ("flow-time");/* Get current time */
        F_PROFILE (f, thread, p) = 0.0469 * (t^2);
        }
    end_f_loop (f, thread)
}
```

The release process of toxic asphyxiant gas was realized by a fixed source term. Studies have shown that, after coal reaches its ignition point (673 K), the CO_2 concentration of the outlet reaches a maximum of about 350,000 ppm, and the CO concentration reaches a maximum of about 60,000 ppm [34]. In this paper, the stable release of flue gas was achieved by setting CO and CO_2 gas inlets at the fire source.

2.2. Control Equation. The high-temperature smoke spreading process in roadway fire is a complex three-dimensional unsteady fluid flow including heat and mass transfer. The numerical simulation satisfies the following conservation equations.

(1) Continuity equation [35]:

$$\frac{\partial \rho}{\partial t} + \frac{\partial (\rho u_i)}{\partial i} = 0. \tag{2}$$
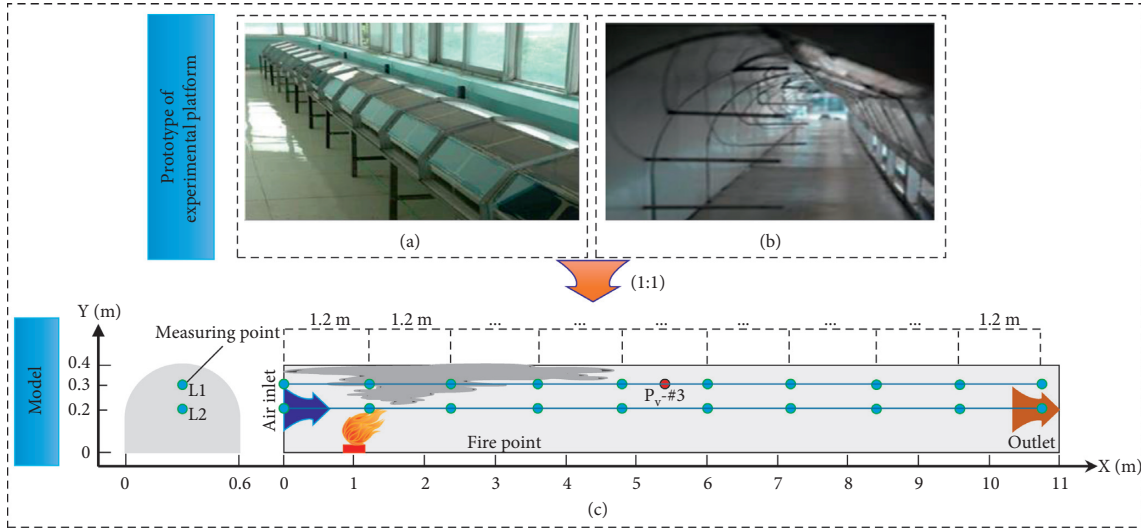
FIGURE 1: Model of roadway. (a) Appearance of the experimental platform. (b) Internal of the experimental platform. (c) Physical model size of the experimental platform.

In the formula, ρ is the fluid density, t is the time, and u_i is the velocity component of the velocity vector u in the direction of i.

(2) Momentum conservation equation [36, 37]:

$$\frac{\partial(\rho u_i)}{\partial t} + \mathrm{div}(\rho u_i u) = \mathrm{div}(\mu\, gradu_i) - \frac{\partial P}{\partial i} + S_i, \quad (3)$$

where μ is the dynamic viscosity (absolute viscosity), S_i is the generalized source term in the direction of i, and $gradu_i$ is the velocity gradient in the direction of i.

(3) Energy conservation equation [28]:

$$\frac{\partial(\rho c_j)}{\partial t} + \mathrm{div}(\rho u T) = \mathrm{div}\left(\frac{a}{c_P}\, gradT\right) + S_T, \quad (4)$$

where T is the temperature of the microelement, a is the heat transfer coefficient of the fluid, c_p is the specific heat capacity of the fluid, and S_T is the viscous dissipation term, including the internal heat source of the fluid and the heat energy generated by the viscous interaction. At the fire source location, S_T is the fire source power source term including the t^2 model in equation (1).

(4) Component mass conservation equation [38]:

$$\frac{\partial(\rho c_j)}{\partial t} + \mathrm{div}(\rho u c_j) = \mathrm{div}(D_j\mathrm{grad}(\rho c_j)) + S_j, \quad (5)$$

where c_i is the volume fraction of component i in the fluid, D_i is the diffusion coefficient of component i in the fluid, and S_i is the volume fraction i in unit time. At the fire source, S_j is the fixed source term of CO and CO_2.

(5) Turbulence equation: incompressible fire smoke flows in the tunnel as a three-dimensional turbulent flow processes, in which the governing equations of the fluid area and the three-dimensional flux in the unsteady and turbulent state were the time-averaged mass Navier–Stokes combined with the k-e realizable model [39, 40]. In the simulation process, the standard k-epsilon turbulence model equation can be used to describe, including the turbulent kinetic energy equation and the turbulent dissipation rate equation, as shown in equations (6) and (7), respectively:

$$\rho\frac{D_k}{D_t} = \frac{\partial}{\partial_{xi}}\left[\left(\mu + \frac{\mu_t}{\sigma_k}\right)\frac{\partial_k}{\partial_{xi}}\right] + G_k + G_b - \rho\varepsilon, \quad (6)$$

$$\rho\frac{D_\varepsilon}{D_t} = \frac{\partial}{\partial_{xi}}\left[\left(\mu + \frac{\mu_t}{\sigma_\varepsilon}\right)\frac{\partial_\varepsilon}{\partial_{xi}}\right]$$
$$+ C_{1\varepsilon}\frac{\varepsilon}{k}(G_k + C_{3\varepsilon}G_b) - C_{2\varepsilon}\rho\frac{\varepsilon^2}{k}, \quad (7)$$

where k is the turbulent kinetic energy, ε is the dissipation rate, xi is the three-dimensional direction, μ_t is the turbulent viscosity coefficient, σ_k is the turbulent Prandtl number of the turbulent kinetic energy equation, 1.0, G_k is the average velocity gradient turbulent kinetic energy, G_b is the turbulent kinetic energy generated by buoyancy, σ_ε is the turbulent Prandtl number of the turbulent dissipation rate equation, 1.3, and $C_{1\varepsilon} = 1.44$ and $C_{2\varepsilon} = 1.92$, $C_{3\varepsilon}$ depend on the velocity component parallel to the direction of gravity and perpendicular to the relationship between the velocity component in the direction of gravity.

2.3. Boundary Conditions' Setting

2.3.1. Assumptions. A fire in a mine roadway is an extremely complex and rapidly developing physicochemical reaction process that generates a large amount of high-temperature flue gas in the roadway. This gas flows turbulently, resulting in unsteady heat and mass transfers. It is especially difficult

to carry out comprehensive numerical simulation of the development and change pattern of mine fire according to the actual physical phenomena in the fire combustion process. Therefore, the combustion model needs to be reasonably simplified. Based on previous research, our simulation used the following assumptions [24, 41]:

(1) The air flow in the roadway is regarded as an ideal gas, ignoring the impact of the air heat expansion in the lane, and no chemical reaction occurs between the gas components there

(2) Assuming that the roadway model is a horizontal smooth roadway, the wall of the roadway is regarded as one with adiabatic constant temperature, no slippage, the air velocity and temperature at the inlet are not affected by the fire, and both the wall and inlet air flow temperature are 293 K

(3) The main components of the smoke generated by fire are CO and CO_2, and other toxic gases are not considered

(4) During the development of the fire, the location of the fire source does not move, and the shape of the tunnel remains intact without deformation

(5) Assuming that all the heat in the fire process comes from the heat source model, no other heat is generated, and there is no mass loss of products

2.3.2. Boundary Conditions and Parameter Settings. The numerical simulation is a transient calculation. In the simulation calculation, an open energy model, the RNG k-epsilon (2-equ) turbulence model, was chosen, and gravity and buoyancy effects were considered. Species model selects species transportation model and opens the P1 radiation model.

The initial temperature of the fire source is set to 673 K.

The inlet boundary condition was set as a velocity inlet, and the inlet air flow temperature was set to 298 K. Research shows that the optimum wind speed to promote the development of fire is 0.4 m/s in the same size test-bed [42]. Therefore, the air velocity value was selected at the entrance boundary. The turbulence intensity was 4.15%, and hydraulic diameter was 0.73 m. The boundary conditions of the air outlet were set to fully develop the outflow. The wall of roadway is a nonslip wall and surface velocity and diffusion coefficient were set to zero regardless of wall penetration. The SIMPLE pressure-velocity coupling method is used to solve the problem iteratively.

2.4. Grid Determination and Model Validation

2.4.1. Grid Determination. In roadway fire simulation, the grid size needed to be reasonably selected according to computer resources and fire characteristic parameters, and the fire source characteristic size D^* was the most relevant and important parameter [43]. Scholars have conducted a series of research on grid rules; for example, Hwang and Edwards [44] used a grid size of 0.06 D^*–0.12 D^* for fire simulation, and the

result is scientific and reasonable. Li [45] considered a grid size of 0.075 D^* can satisfy the calculation conditions after analyzing the grid size accuracy. D^* can be calculated by

$$D^* = \left(\frac{Q}{\rho_0 C_p T_a \sqrt{g}} \right)^{2/5}, \tag{8}$$

where Q is the heat release power, KW, ρ_0 is the air density, $\rho_0 = 1.2043\ kg/m^3$, when the temperature is 293 K, C_p is the constant pressure specific heat, $C_p = 1.004\ KJ/(Kg·K)$, T_a is the ambient temperature, 293 K, and g is the acceleration of gravity, 9.81 m/s². When the calculation time is 60 s, according to formula (1), the heat release rate of the fire source reaches 168.84 KW, and D^* is 0.47 m. Therefore, according to the above scholars' research results, the grid size reaches 0.075 D^* = 0.035 m which can be required in the calculation. Combined with computer performance, this paper chose a grid size of 0.01 m to calculate the result. In addition, the grid is encrypted at the fire source location, and the expansion layer is added at the tunnel wall, as shown in Figure 2. The minimum size of the grid after partial densification was 3.97×10^{-5}m, and the whole grid model contained 654,060 cells.

2.4.2. Model Validation and Calculation Time Determination. The continuity is set in the numerical simulation process, the convergence criteria of k and epsilon are both set to 10^{-5}, the convergence criteria of other variables are set to 10^{-3}, the calculation time step is 0.1 s, the number of time steps is 600, and the simulation result is verified. Since few reports on tunnel fire experiments on the t^2 model and the t^2 fire source power model was a function of time, the heat release was not affected by other variables. Therefore, refer to the experimental test method in [42], which has set the fire source as a stable fire source of 3.14 KW, and other parameters were calculated to prove the correctness of the parameter settings in the model. The corresponding point (define the point as P_v-#3) with the measuring point #3 (5.4 m from the air inlet, 0.3 m height) of the experimental platform in the physical model to compare the results is selected. Through monitoring, the numerical simulation results of measuring point P_v-#3 at different times are obtained, as shown in Figure 3. It can be seen that the numerical simulation results are in good agreement with the experimental results. In the initial stage, the temperature rises slowly and starts to rise rapidly at 15 s; meanwhile, the growth rate of the simulation results is higher than that of experiment. The final temperature is stable at 301–301.5 K, and the results of simulation are higher than that of experiment as a whole, which may be caused by the heat loss of high-temperature smoke flow in the experimental process. The comparison shows that the model can better reflect the flow characteristics of the smoke flow in roadway and meet the basic requirements of roadway fire risk area division.

Through simulation calculation, under the calculation time of 60 s, the high-temperature flue gas can fill the entire tunnel. Consider the evacuation of people during the mine tunnel fire,
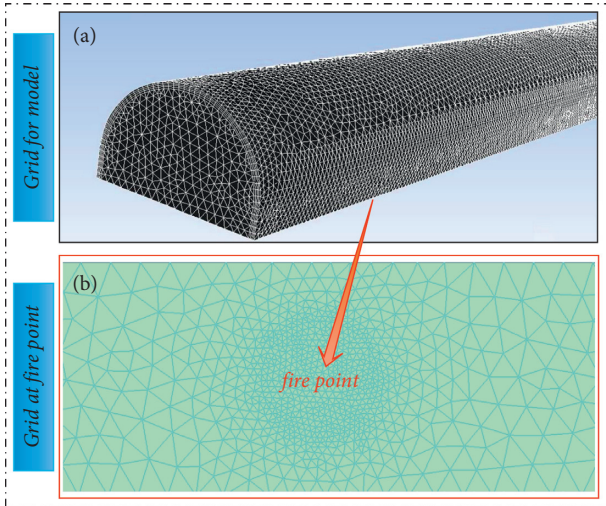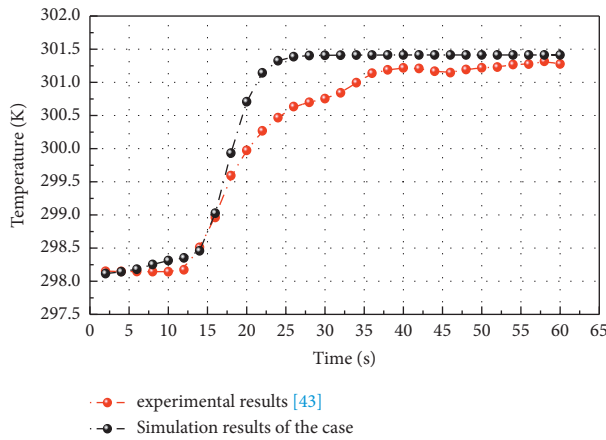
FIGURE 2: Mesh generation.

FIGURE 3: Comparison of simulation and experimental results (P_v-#3 measuring point).

and the escape time of miners should be considered when determining the numerical simulation calculation time. In [46], scholars have carried out experiments on the escape speed of people under different roadway types, slopes, and cross-section conditions. In addition, based on the experimental results, the model of the escape speed of miners during a mine fire was established. The results are as follows:

$$\begin{cases} V_1 = 2.643 + 0.054S + 0.052A - 0.304R_t, & S < 0, \\ V_2 = 2.879 + 0.057S + 0.056A - 0.333R_t, & S \geq 0, \end{cases} \quad (9)$$

where V_1 and V_2 are the miners' escape speed, m/s, S is the roadway slope, °, A is the tunnel section, m², and R_t is the tunnel type, which including track and trackless types. According to formula (9), combined with the case of this paper and physical similar conditions [10], the maximum escape speed of miners in a straight trackless tunnel was 4.342 m/s, and the escape distance within 60 s was 260.52 m, so the calculation time of 60 s was selected.

3. Results and Discussion

3.1. Distribution of Temperature Field. As the simulation proceeded, the simulated gas flow process was monitored by 10 measurement points at levels L_1 and L_2, and the temperature data at each point were recorded and analyzed. The variation pattern of temperature by roadway length at different time points is shown in Figure 4.

The variation pattern of temperature at level L_1 is shown in Figure 4(a). It can be seen from the figure that the temperature at each measuring point has a similar pattern for each time step over the length of the roadway. The highest temperature is 1.4 m downwind of the fire source, the temperature rises gradually over time, and the highest temperature reaches about 319 K. With a gradual increase in the length of the fire source, the temperature shows a downward trend, and at 10 s and 20 s, the temperature is still low. This is because the heat generated by the fire source in the initial stage has not yet been transmitted to the downwind side, resulting in a temperature change that is not obvious, but a stable heat transfer phase is achieved in 20–30 s of development.

The variation pattern of temperature at level L_2 is shown in Figure 4(b). It can be seen from the figure that the temperature variation of the L_2 horizontal measuring points has a similar pattern. The highest temperature point is 0.4 m downwind from the fire source, and the temperature gradually increases with time. The maximum temperature is about 360 K. With the gradual increase of the length of the fire source, the temperature shows a rapid downward trend, and the temperature drop pattern is obvious at the time of 10 s and 20 s. Again, this is because the heat generated by the fire source in the initial stage has not been transmitted to the downwind side, resulting in only a small temperature change, but stable heat transfer starts at 20–30 s.

A temperature cloud map across the vertical section of the axis of the roadway at different time points is shown in Figure 5. It can be seen that the high-temperature flue gas at the fire source flows upward due to buoyancy, and it is affected by the horizontal wind flow of the roadway so that the flue gas flows along toward the downwind side. The fire pressure and high-temperature smoke generated by the fire disturb the steady wind flow in the roadway and create turbulence. As downwind of the fire source, the horizontal flow is at an acute angle with respect to the top of the roadway. After the flue gas generated by the fire source rises to the top of the roadway, most of the flue gas flows downwind from the fire source, but some flue gas flows along the top of the roadway to the upwind side of the fire source to form a countercurrent flue gas layer. It can be seen that the counterflow length gradually increases with time. After the high-temperature smoke from the fire spreads to the downwind side of the roadway, the average temperature in the roadway gradually increases with time but decreases with increasing distance from the fire source. Since the smoke generated by the fire accumulates near the ceiling along the entire roadway, the flue gas stratifies, expands, and
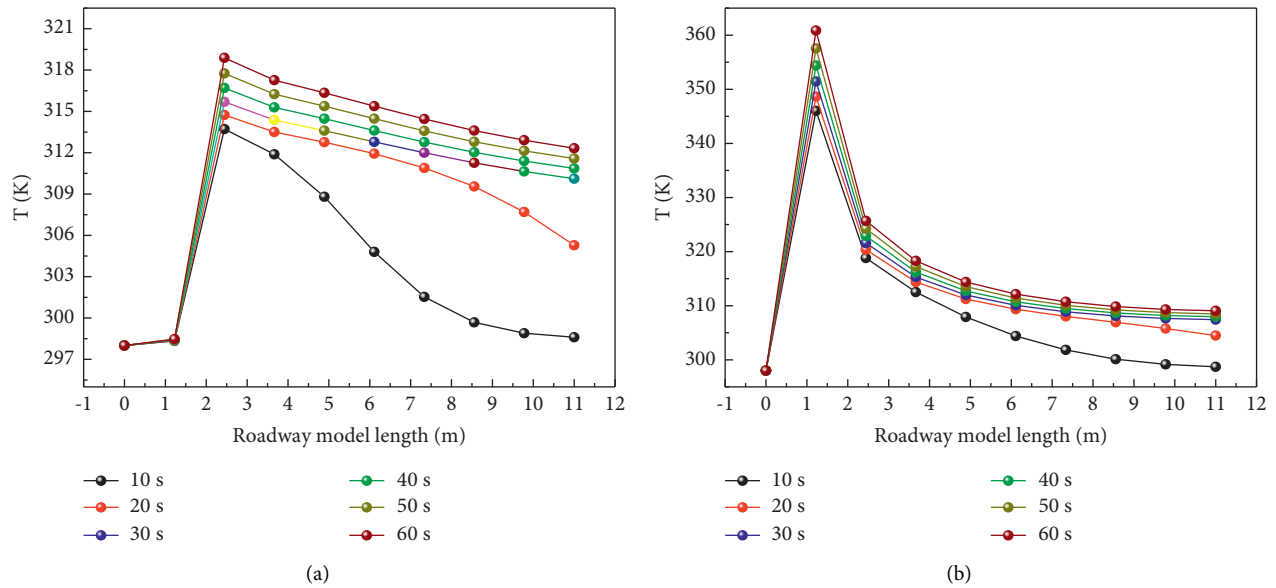
FIGURE 4: Variation pattern of temperature by roadway length at different time points. (a) Level L_1. (b) Level L_2.
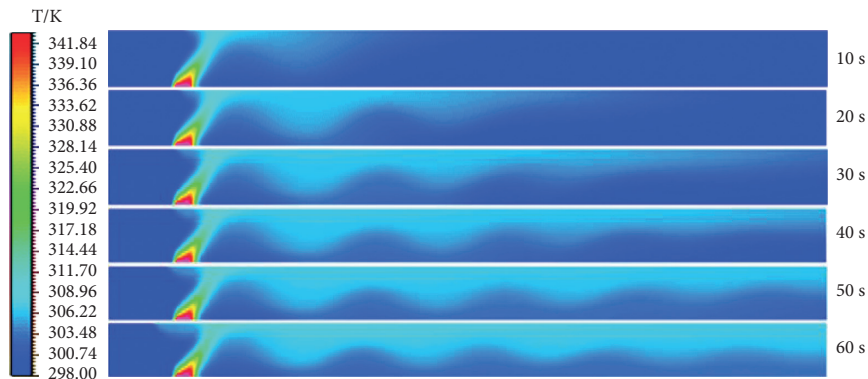

FIGURE 5: Temperature distribution of the vertical section along the roadway axis at different time points.

spreads stably in the roadway, resulting in the temperature of the vertical space of the roadway ranging from high to low, with higher temperatures at the ceiling. It can be seen from the temperature cloud map that the high-temperature wind flow basically spreads along the entire roadway at 30 s, and by 60 s, the outlet temperature reaches 310 K.

3.2. Distribution of Smoke Concentration Field.
During the development of the fire, the smoke generated is entrained by the wind and also spreads along the roadway. Through calculation and postprocessing, the distribution patterns of CO and CO2 gas concentrations in the longitudinal axial planes of the roadway at 10 s, 20 s, 30 s, 40 s, 50 s, and 60 s were obtained, as shown in Figure 6.

It can be seen from Figure 6(a) that the highest CO concentration is about 5% at the source of the fire. During the diffusion of the smoke stream, the CO concentration near the fire source remains basically unchanged and the flue gas generated by the fire diffuses to the roadway ceiling

under the action of buoyancy. As the flue gas continues to diffuse in the wind flow through the roadway, the CO concentration decreases with increasing distance from the fire source. The CO gas concentration contours in the roadway are layered in the horizontal direction. It can be seen from the distribution characteristics of the CO gas concentration contour in the vertical direction that the smoke flows along the top of the roadway due to buoyancy. The CO concentration at the roadway floor is lower than that of the top of the roadway. At about 30 s, smoke from the fire has spread along the entire roadway.

It can be seen from Figure 6(b) that the concentration and variation of CO_2 concentration in the flue gas have a pattern similar to that of CO. The CO_2 concentration at the fire source is the highest, about 30%. The CO_2 concentration near the fire source did not change much during the development of the fire. It can be seen from the contours of CO_2 concentrations that the smoke near the fire source spreads to the top of the roadway due to the heat created by the fire. As with the CO pattern, downwind flow through the
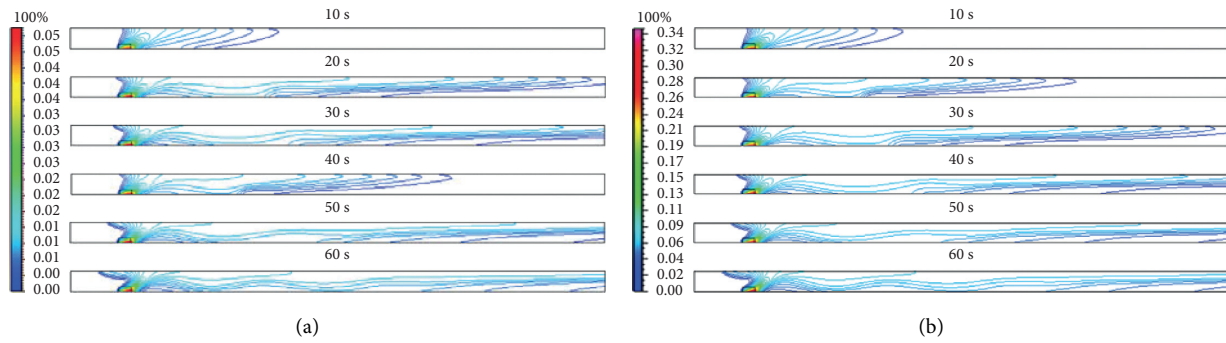
FIGURE 6: Gas contour maps of the vertical section along the roadway axis at different time points. (a) Concentration of CO. (b) Concentration of CO_2.

roadway diffuses the smoke, and the CO_2 concentration gradually decreases as the distance from the fire source increases. In addition, due to buoyancy, the smoke accumulates at the top of the roadway, and the CO_2 gas concentration contour is hierarchically distributed in the vertical direction; at 30 s, the CO_2 is diffused along the entire roadway.

4. Classification of Fire Danger Zones

In a coal mine fire, the fire source will release a large amount of heat and toxic gases. Due to the wind flow, it spreads widely through the limited space of the roadway. After a certain time, the high-temperature flue gas products are gradually distributed throughout the roadway space, certainly forming an oxygen-deficient and poisonous environment, which poses grave danger to the life and safety of underground workers [47]. Therefore, based on the simulation results, the authors used the temperature and toxic gas distribution patterns at the measurement points to classify the fire danger areas of the roadway based on the selected fire risk assessment indicators.

4.1. Assessment Indicators and Threshold Value. The main cause of casualties in mine fire accidents is suffocation and poisoning by high-temperature smoke. Previous survey results showed that among the main combustion products of fire—CO, CO_2, SO_2, and other high-temperature organic gases—the largest cause of casualties is CO and CO_2 in high-temperature flue gas [48]. Therefore, this paper selects the temperature, CO, and CO_2 as indicators. According to the research results of scholars [5, 25, 49–54], the impact of different indexes on human body and critical values are shown in Table 1. According to the degree of influence of high-temperature flue gas on the human body, thresholds were selected to classify risk in the flue gas-spreading area.

4.1.1. Flue Gas Temperature. According to the influence of different temperatures on the human body, 303.15 K, 313.15 K, and 338.15 K are used as the temperature thresholds to classify the danger zone according to heat injury in a mine fire. The downwind side of the roadway was divided into four areas: safe area (I), slightly dangerous area

(II), moderately dangerous area (III), and highly dangerous area (IV). The same classes were used for all three indicators. The specific classification thresholds are shown in Table 2.

4.1.2. CO Concentration. According to the influence of different CO gas concentrations on the human body, 0.005%, 0.32%, and 0.64% are used as the CO concentration thresholds for hazard classification. These thresholds are shown in Table 3.

4.1.3. CO_2 Concentration. Carbon dioxide itself is nontoxic, but it asphyxiates people by displacing oxygen, and it is a major cause of fire casualties, especially in enclosed spaces. Its long-term allowable concentration is 5,000 ppm. According to the influence of different CO_2 gas concentrations on the human body, 0.5%, 3%, and 6% are used as the CO_2 concentration thresholds to create the hazard classifications. The thresholds are shown in Table 4.

4.2. Classification Results of Hazardous Areas

4.2.1. High-Temperature Hazardous Areas. We used the simulation results for the roadway distribution pattern of the flue gas temperature at levels L_1 and L_2 for each time step to draw two critical temperature classification lines at 303.15 K and 313.15 K. Furthermore, the horizontal temperature field danger zone was also classified, and the result is shown in Figure 7.

It can be seen that, during the first 60 s of fire development, the maximum temperature at level L_1 reaches 360 K, which exceeds the critical value of danger class IV. The highest temperature at the L_2 level reaches 320 K, which is within the danger class III range. During this time, both the level L_1 and L_2 locations having danger class I gradually disappear on the downwind side of the fire source and become class II zones.

The critical temperature classification was applied to the results of the roadway horizontal distribution of different high-temperature danger zones at each time step, and the results are shown in Table 5. Among the four danger zones shown in the table, the safe roadway zone is mainly on the upwind side of the fire source during the

TABLE 1: Impact of different indexes on human body and critical values [5, 25, 49–54].

T (K)	Impact on human body	C_{CO} (ppm)	Impact on human body	C_{CO_2} (ppm)	Impact on human body
293.15–301.15	Suitable temperature	<24	Basically no effect	450	About the concentration in the air
301.15–303.15	Feeling hot and slightly uncomfortable	50	Allowable exposure concentration	5000	No symptoms within 6 h
303.15–307.15	Human sweat glands work, sweating a lot, heartbeat, and blood circulation is increased	200	2-3 hours, mild forehead headache	10000–20000	Feel uncomfortable
307.15–313.15	Body surface fever is unbearable and internal heat is difficult to lose	400	1-2 hours, headache, nausea, dizziness afterwards	30000	Stimulate the respiratory center and increase the number of breaths and allowable evacuation concentration
313.15–338.15	High temperature causes dizziness and dysfunction of body temperature regulation	800	45 minutes, strong headache, vomiting; 2 hours, coma	40000	Shortness of breath, headache, rapid heartbeat and other symptoms
338.15–363.15	Tolerable temperature for a short period of time; as the temperature rises, the human center is threatened and the internal circulatory system is disordered	3200	5~10 minutes, headache and dizziness; 30 minutes, no sensation	50000	Difficulty breathing
363.15–393.15	Exceeding the tolerance of the skin, inhaling into the human body will cause blisters in the respiratory trachea and bronchus, and even tissue necrosis	6400	Headache and dizziness within 1~2 minutes; 10~15 minutes, unconsciousness, life-threatening	60000	Shortness of breath, dyspnea
>393.15	Skin burns and irrecoverable, muscle cramps, suffocation, and death prone	12800	Instantaneous loss of consciousness, resulting in death	70000–100000	Lose consciousness after several breaths 1-2 minutes, resulting in death

TABLE 2: Temperature thresholds.

Levels of danger	Temperature range
Safe area(I)	<303.15 K
Slightly dangerous area (II)	303.15 K~313.15 K
Moderately dangerous area (III)	313.15 K~338.15 K
Highly dangerous area (IV)	>338.15 K

TABLE 4: The CO_2 concentration thresholds.

Levels of danger	CO_2 (%)
Safe area (I)	<0.5
Slightly dangerous area (II)	0.5~3
Moderately dangerous area (III)	3~6
Highly dangerous area (IV)	>6

TABLE 3: The CO concentration thresholds.

Levels of danger	CO (%)
Safe area(I)	<0.005
Slightly dangerous area (II)	0.005~0.32
Moderately dangerous area (III)	0.32~0.64
Highly dangerous area (IV)	>0.64

initial fire development (10 s), although a few similar areas exist downwind of the fire source at this time. Two danger class II areas and additional class III areas are distributed downwind of the fire source. As the fire develops, the danger class I areas within the roadway remain essentially unchanged, but the range of danger class II areas is constantly changing.

Figure 8 uses the distribution result for danger level classification of the roadway to illustrate the variation of the high-temperature danger zone range of measurement levels L_1 and L_2 over time. It shows that the area identified danger class I is the largest before 10 s; class I areas are rapidly reduced from 10 s to 20 s, and the size of the danger class II areas increase. After 20 s, the danger class I areas of both levels L_1 and L_2 remained unchanged, but the danger class II area began to decrease linearly with time, with reduction rates of 0.17 m/s and 0.06 m/s for levels L_1 and L_2, respectively. The danger class III areas for levels L_1 and L_2 increased linearly, with growth rates of 0.17 m/s and 0.05 m/s, respectively, and the linear growth rate of the danger class IV area of level L_2 was 0.01 m/s. In general, the unsafe area determined by the L_1 horizontal temperature is larger than that determined by level L_2.

4.2.2. Smoke Spread Danger Zone. All the gaseous components of the flue gas lead to poisonous asphyxiation and death. Therefore, when smoke spreads through the roadway, it is necessary to evaluate both the CO and CO_2 levels to classify areas with asphyxiation hazards. From the simulation results for smoke spreading, it can be seen that, during the mine fire development, the gas generated by the fire source will gather near the ceiling and spread downwind
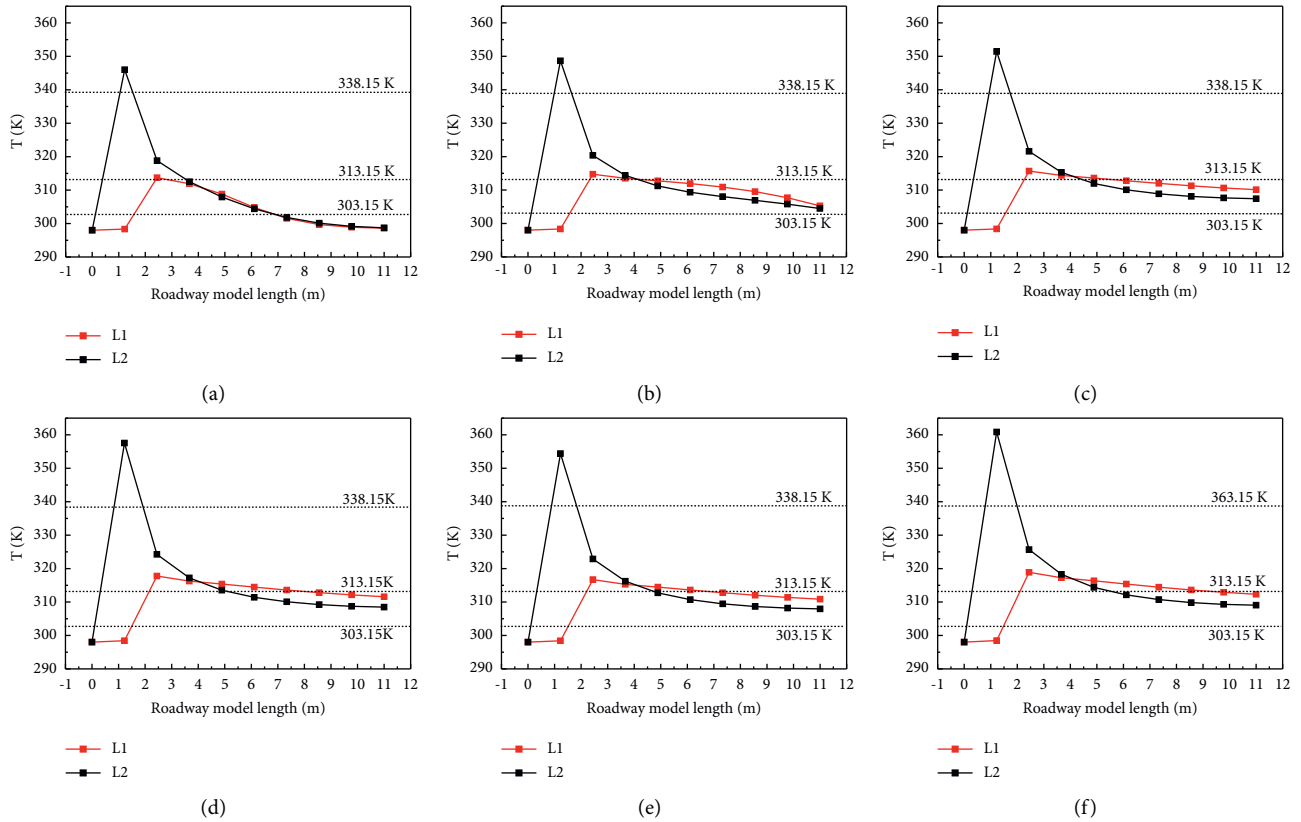
Figure 7: Classified results of horizontal temperature field danger zone. (a) 10 s, (b) 20 s, (c) 30 s, (d) 40 s, (e) 50 s, and (f) 60 s.

Table 5: Results of comprehensive classification of hazardous areas.

Time	Index	Safe area (I) (m)	Slightly dangerous area (II) (m)	Moderately dangerous area (III) (m)	Highly dangerous area (IV) (m)
10 s	L_1	(0,1.6)∪(6.7,11)	(1.6,6.7)	None	None
	L_2	(0,0.2)∪(6.8,11)	(0.2,0.4)∪(3.6,6.8)	(0.4,1)∪(1.5,3.6)	(1,1.5)
20 s	L_1	(0,1.6)	(1.6,2.4)∪(4.2,11)	(2.4,4.2)	None
	L_2	(0,0.1)	(0.1,0.4)∪(4.2,11)	(0.4,1)∪(1.6,4.2)	(1,1.6)
30 s	L_1	(0,1.6)	(1.6,2.3)∪(5.5,11)	(2.3,5.5)	None
	L_2	(0,0.1)	(0.1,0.4)∪(4.5,11)	(0.4,1)∪(1.7,4.5)	(1,1.7)
40 s	L_1	(0,1.6)	(1.6,2.2)∪(6.8,11)	(2.2,6.8)	None
	L_2	(0,0.1)	(0.1,0.4)∪(4.8,11)	(0.4,0.9)∪(1.8,4.8)	(0.9,1.8)
50 s	L_1	(0,1.6)	(1.6,2.2)∪(8.1,11)	(2.2,8.1)	None
	L_2	(0,0.1)	(0.1,0.4)∪(5.2,11)	(0.4,0.8)∪(1.9,5.2)	(0.8,1.9)
60 s	L_1	(0,1.6)	(1.6,2.1)∪(9.5,11)	(2.1,9.5)	None
	L_2	(0,0.1)	(0.1,0.3)∪(5.7,11)	(0.3,0.7)∪(2,5.7)	(0.7,2)

from the fire source, resulting in a higher concentration of CO and CO_2 in the upper part of the tunnel. According to the average height of the miners, combined with the principle of physical similarity [55, 56], the gas concentrations of CO and CO_2 at the L_2 level were selected to classify the dangerous areas in the roadway.

The smoke toxicity risk assessment index was used to draw the line representing the CO and CO_2 concentration curves at the classification thresholds, as shown in Figure 9. It can be seen from Figure 9 that, during fire development, as the CO and CO_2 gases generated by the fire source flowed downwind from the fire source, their concentrations in the roadway gradually increased with time. Areas closer to the fire source experienced greater increases in gas concentration, which rapidly crossed the thresholds for successively more dangerous classifications.

The distribution results were used to classify the smoke danger at each horizontal point of the roadway over time, as shown in Table 6. It can be seen from Table 6 that some areas of the roadway, classified as toxic according to CO and CO_2 hazard, are coincident. Therefore, in the final result determination, the CO and CO_2 gas toxicity classification results were combined and further divided based on the results of the high toxicity level.

(a)   (b)
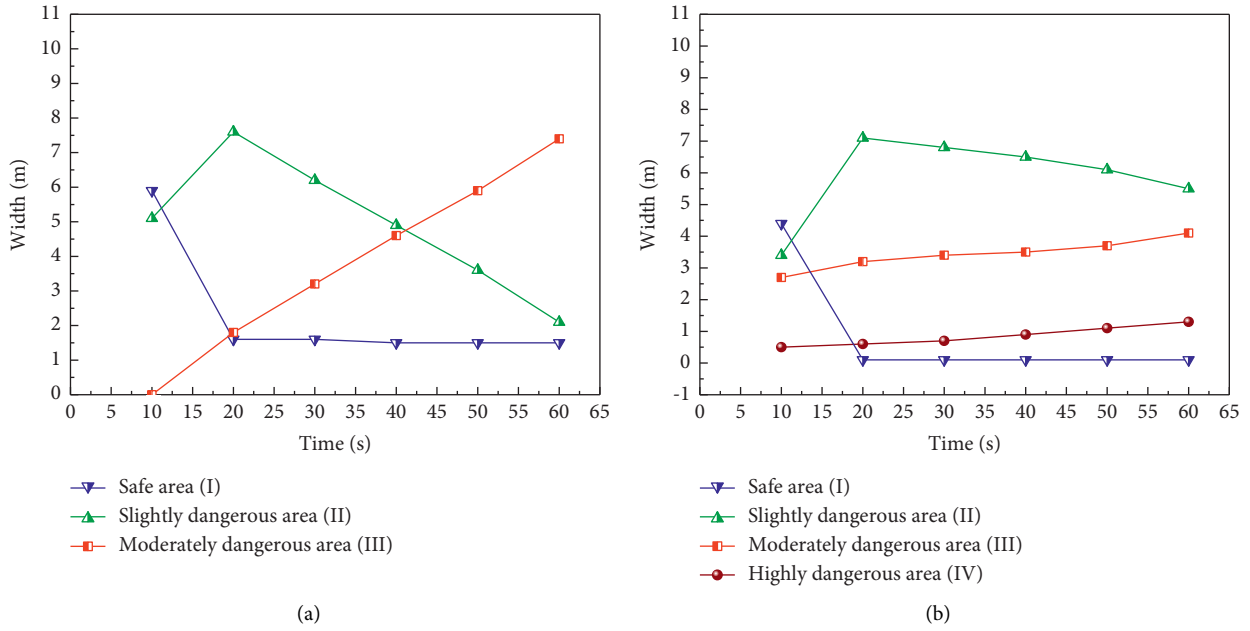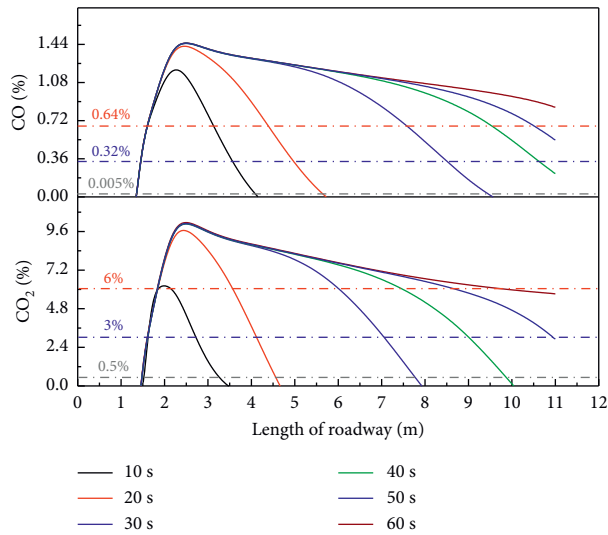
FIGURE 8: The variation of the high-temperature danger zone range over time. (a) L_1, (b) L_2.

FIGURE 9: Distribution of CO and CO_2 gas concentrations at L_2.

TABLE 6: Classification results of different smoke danger zones.

Time	Index	Safe area (I) (m)	Slightly dangerous area (II) (m)	Moderately dangerous area (III) (m)	Highly dangerous area (IV) (m)
10 s	CO	(0,1.3)∪(4.2,11)	(1.3,1.5)∪(3.6,4.2)	(1.5,1.6)∪(3.2,3.6)	(1.6,3.2)
	CO_2	(0,1.5)∪(3.3,11)	(1.5,1.6)∪(2.7,3.3)	(1.6,1.8)∪(2.2,2.7)	(1.8,2.2)
20 s	CO	(0,1.3)∪(5.7,11)	(1.3,1.5)∪(5,5.7)	(1.5,1.6)∪(4.4,5)	(1.6,4.4)
	CO_2	(0,1.5)∪(4.6,11)	(1.5,1.6)∪(4.1,4.6)	(1.6,1.8)∪(3.6,4.1)	(1.8,3.6)
30 s	CO	(0,1.3)∪(9.5,11)	(1.3,1.5)∪(8.5,9.5)	(1.5,1.6)∪(7.6,8.5)	(1.6,7.6)
	CO_2	(0,1.5)∪(7.8,11)	(1.5,1.6)∪(7.1,7.8)	(1.6,1.8)∪(6,7.1)	(1.8,6)
40 s	CO	(0,1.3)	(1.3,1.5)∪(10.6,11)	(1.5,1.6)∪(9.6,10.6)	(1.6,9.6)
	CO_2	(0,1.5)∪(9.9,11)	(1.5,1.6)∪(9,9.9)	(1.6,1.8)∪(7.5,9)	(1.8,7.5)
50 s	CO	(0,1.3)	(1.3,1.5)	(1.5,1.6)∪(10.6,11)	(1.6,10.6)
	CO_2	(0,1.5)	(1.5,1.6)∪(10.9,11)	(1.6,1.8) ∪(8.7,10.9)	(1.8,8.7)
60 s	CO	(0,1.3)	(1.3,1.5)	(1.5,1.6)	(1.6,11)
	CO_2	(0,1.5)	(1.5,1.6)	(1.6,1.8)∪(9.8,11)	(1.8,9.8)

TABLE 7: Results of risk classification of smoke poisoning.

Time	Safe area (I) (m)	Slightly dangerous area (II) (m)	Moderately dangerous area (III) (m)	Highly dangerous area (IV) (m)
10 s	(0,1.3)∪(4.2,11)	(1.3,1.5)∪(3.6,4.2)	(1.5,1.6)∪(3.2,3.6)	(1.6,3.2)
20 s	(0,1.3)∪(5.7,11)	(1.3,1.5)∪(5,5.7)	(1.5,1.6)∪(4.4,5)	(1.6,4.4)
30 s	(0,1.3)∪(9.5,11)	(1.3,1.5)∪(8.5,9.5)	(1.5,1.6)∪(7.6,8.5)	(1.6,7.6)
40 s	(0,1.3)	(1.3,1.5)∪(10.6,11)	(1.5,1.6)∪(9.6,10.6)	(1.6,9.6)
50 s	(0,1.3)	(1.3,1.5)	(1.5,1.6)∪(10.6,11)	(1.6,10.6)
60 s	(0,1.3)	(1.3,1.5)	(1.5,1.6)	(1.6,11)

The results of the reclassification are shown in Table 7. It can be seen from Table 7 that, in the development stage of a mine fire, the toxic environment in the roadway can be divided into four areas. In the early stage of the fire, the safe area in the roadway is mainly on the upwind side of the fire source and the roadway exit. As the fire continues to develop, the flue gas spreads to the downwind side, resulting in a gradual increase in the risk level throughout the tunnel, and the danger class II area is distributed on the downwind side of the fire source. As the fire develops, the safety zone in the roadway remains basically unchanged for more than 30 s, but the range of the more hazardous areas is constantly changing.

The result of the classification was processed to view how the range of the danger zone of the roadway changes over time, as shown in Figure 10. As can be seen from Figure 10, the safe area of the roadway is the largest before 25 s. With the development of the fire, the safe area downwind of the fire source rapidly shrinks over time, and the range of areas with danger classes II and III are initially small and then increase and decrease with time, with a small rate of change. The range of danger class IV increases rapidly at first, and then, its growth rate slows. The change of the range of danger class I and IV has obvious regularity. The following relationship between the range and time of the dangerous areas is obtained by fitting:

$$X_D = \begin{cases} 1.2 + \dfrac{7.1}{1 + 10^{-0.1(24.8-t)}}, & \text{(I)}, \\[3mm] \dfrac{9.6}{1 + e^{0.1(26.2-t)}}, & \text{(IV)}, \end{cases} \tag{10}$$

where X_D is the is the length of the danger area, m, and t is time, s.

4.3. Results of Comprehensive Analysis on Hazardous Areas.
As mine fires develop, the amount of generated heat and smoke increases greatly, and the safe areas in the roadways are simultaneously threatened by high temperatures and toxins. During the fire development process, the unsafe (class II) high-temperature area of the roadway near the tunnel ceiling (level L_1) is larger than that at the middle height of the tunnel (level L_2). The horizontal high-temperature class II area range linearly decreases over time, with a reduction rate of 0.17 m/s, and the class III area range increases linearly at a rate of 0.17 m/s.

However, compared with the high-temperature danger areas, the toxicity of the flue gas creates larger areas with
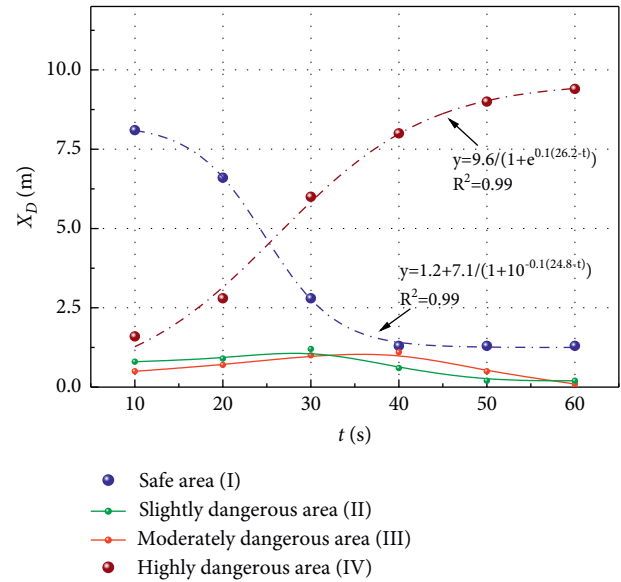

FIGURE 10: Variation law of the dangerous area range over time.

higher danger classification zones. The area safe from a toxic atmosphere shrinks rapidly over time, from 0.15 m/s to 0.38 m/s. The areas with danger classes II and III are small, and the most dangerous class IV area grows rapidly, up to 0.32 m/s.

5. Conclusions

The numerical simulation results show that, during the mine fire in a straight roadway, the temperature and gas concentration form a gradient from high to low in the downward vertical direction, and part of the flue gas flows along the top of the roadway toward the upwind side of the fire source to form a flue gas counterflow. The numerical simulation results are in good agreement with the experimental results of relevant scholars.

In this study, the temperature and toxicity of flue gas are taken as evaluation indexes, and the risk assessment of flue gas temperature and toxicity is carried out according to the harm degree of different indexes to human body. Based on previous research foundations, the classification standards of dangerous areas were further excavated, and the critical value of classification of dangerous areas was determined, and the smoke spread area was divided into four classifications, ranging from safe (I) to highly dangerous (IV).

During fire development, areas made unsafe by high temperatures are larger near the tunnel ceiling (level L_1) than

those at the middle height (level L_2). The danger class II area at level L_1 linearly decreased over time, and the area with danger class III increased linearly. Compared with the range of high-temperature danger areas, areas with dangerous levels of toxic flue gas were larger and more dangerous. Combined with high-temperature and toxic gas index, the relationship between the range of dangerous area and time is determined.

Through the research of numerical simulation, the idea and method are provided for the division of dangerous area and the judgment of rescue danger of mine tunnel fire. According to the numerical simulation results and the physical similarity simulation criteria, the dangerous area of the roadway during the mine fire under actual site conditions can be calculated. However, because the simulation in this paper is based on the calculation model established by the small-scale tunnel fire experiment platform, there may be some deficiencies in the results of physical similarity calculation, which needs to be further improved in the future research.

Data Availability

The data used to support the findings of this study are available from the corresponding author upon request.

Conflicts of Interest

The authors declare that there are no conflicts of interest regarding the publication of this paper.

Authors' Contributions

The study was carried out in collaboration with all authors. All authors have read and approved the final manuscript.

Acknowledgments

References

[1] C. G. Fan, X. Y. Li, Y. Mu, F. Y. Guo, and J. Ji, "Smoke movement characteristics under stack effect in a mine laneway fire," *Applied Thermal Engineering*, vol. 110, pp. 70–79, 2017.

[2] X. Q. Shi, Y. T. Zhang, X. K. Chen, and Y. B. Zhang, "Effects of thermal boundary conditions on spontaneous combustion of coal under temperature-programmed conditions," *Fuel*, vol. 295, Article ID 120591, 2021.

[3] Y. Liu, H. Wen, J. Guo, Y. Jin, G. Wei, and Z. Yang, "Coal spontaneous combustion and N2 suppression in triple goafs: a numerical simulation and experimental study," *Fuel*, vol. 271, p. 117625, 2020.

[4] V. Babrauskas, R. G. Gann, B. C. Levin et al., "Methodology for obtaining and using toxic potency data for fire hazard analysis," *Fire Safety*, vol. 31, no. 4, pp. 345–358, 1998.

[5] W. F. Shi, *The Numerical Models Research on Mine Fire Smoke Flow and Regularities of Temperature Distribution"*, Taiyuan University of Technology, Taiyuan, China, 2013.

[6] J. Guo, H. Wen, X. Z. Zheng, Y. Liu, and X. J. Cheng, "A method for evaluating the spontaneous combustion of coal by monitoring various gases," *Process Safety and Environmental Protection*, vol. 126, pp. 223–231, 2019.

[7] G. T. Atkinson and Y. Wu, "Smoke control in sloping tunnels," *Fire Safety Journal*, vol. 27, pp. 335–341, 1996.

[8] Z. X. Li, J. X. Yu, and S. K. Lin, "Simulation of wind resistance drift in mine ventilation system during fire," *Journal of Safety and Environment*, vol. 11, pp. 172–175, 2011.

[9] J. Deng, Y. Xiao, and Q. Li, "Experimental studies of spontaneous combustion and anaerobic cooling of coal," *Fuel*, vol. 157, pp. 261–269, 2015.

[10] W. K. Chow, Y. Gao, J. F. Zou, Q. K. Liu, C. L. Chow, and L. Miao, "Numerical studies on thermally-induced air flow in sloping tunnels with experimental scale modelling justifications," *Fire Technology*, vol. 54, pp. 867–892, 2018.

[11] J. Guo, Y. Liu, X. J. Cheng, H. Yan, and Y. Q. Xu, "A novel prediction model for the degree of rescue safety in mine thermal dynamic disasters based on fuzzy analytical hierarchy process and extreme learning machine," *International Journal of Heat and Technology*, vol. 36, no. 4, pp. 1336–1342, 2018.

[12] H. Wen, Y. Liu, J. Guo, Y. F. Jin, and X. Z. Zheng, "A multi-index-classified early warning method for spontaneous combustion of coal under air leakage blocking," *International Journal of Oil, Gas and Coal Technology*, vol. 27, no. 2, pp. 208–226, 2020.

[13] NFPA 264, *Standard Method of Test for Heat and Visible Smoke Release Rates for Material and Produces Using an Oxygen Consumption Calorimeter*, American National Fire Protection Association, Quincy, MA, USA, 1992.

[14] J. Zhu, R. Huo, and Y. S. Fu, "Experimental study of smoke movement in the vertical shaft," *Journal of China University of Mining & Technology*, vol. 36, pp. 603–608, 2007.

[15] S. G. Zhang, H. Yang, Y. Z. Yao et al., "Numerical investigation of back-layering length and critical velocity in curved subway tunnels with different turning tadius," *Fire Technology*, vol. 53, pp. 1765–1793, 2017.

[16] P. Xu, S. P. Jiang, R. J Xing, and J. Q. Tan, "Full-scale immersed tunnel fire experimental research on smoke flow patterns," *Tunnelling and Underground Space Technology*, vol. 81, pp. 494–505, 2018.

[17] M. R. Egan, "Impact of air velocity on the development and detection of small coal fires," *Bureau of Mines Report of Investigations*, vol. 9480, pp. 1–15, 1993.

[18] S. R. Li, *Study on the Influence of Moving Fire Source on Tunnel Temperature Field Distribution and Smoke Flow*, Xi'an University of Science and Technology, Xi'an, China, 2013.

[19] Y. Z. Li and H. Ingason, "Influence of fire suppression on combustion products in tunnel fires," *Fire Safety Journal*, vol. 97, pp. 96–110, 2018.

[20] S. Shafee and A. Yozgatligil, "An experimental study on the burning rates of interacting fires in tunnels," *Fire Safety Journal*, vol. 96, pp. 115–123, 2018.

[21] K. Li, J. Quan, and C. F. Yu, "Influence of fire location on ventilation and secondary disasters in roadway excavation," *Journal of Tsinghua University*, vol. 50, pp. 270–273, 2010.

[22] K. Zhu, Y. Z. Yao, S. G. Zhang, H. Yang, R. F. Zhang, and X. D. Cheng, "Smoke movement in a sloping subway tunnel under longitudinal ventilation with blockage," *Fire Technology*, vol. 53, pp. 1985–2006, 2017.

[23] A. Vaitkevicius and R. Carvel, "Investigating the throttling effect in tunnel fires," *Fire Technology*, vol. 52, pp. 1619–1628, 2016.

[24] L. He, Z. S. Xu, H. G. Chen, Q. L. Liu, Y. X. Wang, and Y. Zhou, "Analysis of entrainment phenomenon near mechanical exhaust vent and a prediction model for smoke temperature in tunnel fire," *Tunnelling and Underground Space Technology*, vol. 80, pp. 143–150, 2018.

[25] L. Chen, C. F. Wu, Z. Y. Chen, L. J. Zhou, and Q. L. Deng, "Numerical simulation study on the regional division of mine roadways fire safety," *Fire Science and Technology*, vol. 35, no. 5, pp. 633–636, 2016.

[26] K. Wang, S. G. Jiang, W. Q. Zhang, Z. Y. Wu, and W. Shao, "Numerical simulation and application research of mine fire emergency rescue system," *Journal of China Coal Society*, vol. 37, pp. 857–862, 2012.

[27] V. Babrauskas, R. G. Gann, and B. C. Levin, "Toxic potency measurement for fire hazard analysis," *Fire Technology*, vol. 28, no. 2, pp. 163–167, 1992.

[28] K. Wang, S. Jiang, X. P. Ma et al., "Numerical simulation and application study on a remote emergency rescue system during a belt fire in coal mines," *Natural Hazards*, vol. 84, pp. 1463–1465, 2016.

[29] W. W. Jones, G. P. Forney, R. D. Peacock, and P. A. Reneke, *A Technical Reference for CFAST: An Engineering Tool for Estimating Fire and Smoke Transport, NIST TN 1431*, pp. 17–77, National Institute of Standards and Technology, Gaithersburg, MD, USA, 2000.

[30] Y. P. Cheng, L. Chen, and M. J. Zhang, "The models and experimental testing method of heat release rate of fuel during the development of fire," *Fire Safety Science*, vol. 11, no. 2, pp. 70–74, 2002.

[31] S. He, *On Application of Instable Fire to Network Model of Fire and the Performance-Based Design on the Smoke Control System*, Chongqing University, Chongqin, China, 2006.

[32] L. M. Zheng, *ANSYS Fluent 15.0: Fluid Computing from Initial to Proficient*, Publishing House of Electronics Industry, Beijing, China, 2015.

[33] Z. Zhang, *Simulation and Division of Danger Areas of Smoke Flow of Belt Fire in Coal Mine*, Xi'an University of Science and Technology, Xi'an, China, 2017.

[34] Y. F. Jin, J. Guo, and H. Wen, "Experimental study on characteristics of high temperature oxygen-depleted oxidation combustion of coal spontaneous combustion," *Journal of China Coal Society*, vol. 40, pp. 596–602, 2015.

[35] G. Zhou, W. M. Cheng, R. Zhang et al., "Numerical simulation and disaster prevention for catastrophic fire airflow of main air-intake belt roadway in coal mine—a case study," *Journal of Central South University*, vol. 22, no. 6, pp. 2359–2368, 2015.

[36] J. Shen, H. Q. Zhu, M. G. Luo, and D. L. Liu, "Numerical simulation of CO distribution discharged by flame-proof vehicle in underground tunnel of coal mine," *Journal of Loss Prevention in the Process Industries*, vol. 40, pp. 117–121, 2016.

[37] X. Q. Shi, Y. T. Zhang, X. K. Chen, Y. B. Zhang, and T. Ma, "Numerical study on the oxidation reaction characteristics of coal under temperature-programmed conditions," *Fuel Processing Technology*, vol. 213, Article ID 106671, 2020.

[38] H. Wen, Y. Liu, Y. F. Jin et al., "Numerical simulation for mine oblique lane fire based on PDF non-premixed combustion," *Combustion Science and Technology*, vol. 193, pp. 90–109, 2019.

[39] B. E. Launder and D. B. Spalding, "The numerical computation of turbulent flows," *Computer Methods in Applied Mechanics and Engineering*, vol. 3, pp. 269–289, 1974.

[40] M. Musto and G. Rotondo, "Numerical comparison of performance between traditional and alternative jet fans in tiled tunnel in emergency ventilation," *Tunnelling and Underground Space Technology*, vol. 42, pp. 52–58, 2014.

[41] H. Y. Niu, C. L. Qiao, J. Y. An, and J. Deng, "Experimental study and numerical simulation of spread law for fire on tunnel," *Journal of Central South University of Technology*, vol. 22, pp. 701–706, 2015.

[42] J. Guo, Y. Liu, Y. F. Jin, X. Z. Zheng, and Z. Zhang, "Spatiotemporal evolution law of multiple parameters of roadway environment for rubber-belt fire in mine," *Journal of Xi'an University of Science and Technology*, vol. 39, pp. 21–27, 2019.

[43] K. McGrattan, S. Hostikka, R. McDermott et al., *Overholt. Fire Dynamics Simulator User's Guide (Version 6)*, National Institute of Standards and Technology, Gaithersburg, MA, USA, 2018.

[44] C. C. Hwang and J. C. Edwards, "The critical ventilation velocity in tunnel fires-a computer simulation," *Fire Safety Journal*, vol. 40, pp. 213–244, 2005.

[45] Y. Z. Li, *Study of Fire Characteristics and Smoke Control in Super Long Tunnels with Rescue Stations*, Southwest Jiaotong University, Chengdu, China, 2010.

[46] R. X. Zhang, R. S. Nie, H. Z. Zhao, and Y. Q. Fan, "Experimental study on the escape velocity of minersduring mine fire periods," *Mathematical Problems in Engineering*, vol. 2018, Article ID 9458785, 2018.

[47] Y. Y. Yan and Z. G. Jiang, "Simulation of smoke movement in mine roadway fire," *Mining Safety & Environmental Protection*, vol. 5, pp. 13-14+26, 2007.

[48] GB5044-85, *Occupational Exposure Hazard Classification*, China Standard Press, Beijing, China, 2009.

[49] K. Wang, S. G. Jiang, X. P. Ma et al., "Information fusion of plume control and personnel escape during the emergency rescue of external-caused fire in a coal mine," *Process Safety and Environmental Protection*, vol. 103, pp. 46–59, 2016.

[50] A. Löhnert, N. Monreal, C. Knaust, A. Hofmann, and U. Krause, "CFD modeling approach of smoke toxicity and opacity for flaming and non-flaming combustion processes," *Fire and Materials*, vol. 40, no. 6, pp. 759–772, 2015.

[51] NFPA, *Carbon Monoxide Risks at Home Fact Sheet*, National Fire Protection Association, Quincy, MA, USA, 2000, http://www.nfpa.org.

[52] C. Ye, Y. Liu, C. Sun, Y. Q. Jiang, and B. Wang, "Simulation study on personnel evacuation considering impacts of fire products," *China Safety Science Journal*, vol. 30, no. 6, pp. 142–151, 2020.

[53] C. Q. Du, *Effect of Temperature Variation on Human Thermal Regulation and Health and its Molecular Mechanism*, Chongqing University, Chongqing, China, 2018.

[54] State Administration of Work Safety and National Mine Safety Administration, *Coal Mine Safety Regulations (2016)*, Coal Industry Press, Beijing, China, 2016.

[55] Y. Zeng, K. Liu, X. Zhou, and L. Fan, "Tunnel temperature fields analysis under the couple effect of convection-conduction in cold regions," *Applied Thermal Engineering*, vol. 120, pp. 378–392, 2017.

[56] A. Li, Y. Zhang, J. Hu, and R. Gao, "Reduced-scale experimental study of the temperature field and smoke development of the bus bar corridor fire in the underground hydraulic machinery plant," *Tunnelling and Underground Space Technology*, vol. 41, pp. 95–103, 2014.